Bond-slip model for FRP laminates externally bonded to concrete at elevated temperature

Jian-Guo Dai[1], W.Y. Gao[2] and J.G. Teng[3]

Abstract: This paper presents a nonlinear local bond-slip model for fiber reinforced polymer (FRP) laminates externally bonded to concrete at elevated temperature for future use in the theoretical modeling of fire resistance of FRP-strengthened concrete structures. The model is an extension of an existing two-parameter bond-slip model for FRP-to-concrete interfaces at ambient temperature. The two key parameters employed in the proposed bond-slip model, the interfacial fracture energy G_f and the interfacial brittleness index B, were determined using existing shear test data of FRP-to-concrete bonded joints at elevated temperature. In the interpretation of test data, the influences of temperature-induced thermal stress and temperature-induced bond degradation are properly accounted for. As may be expected, the interfacial fracture energy G_f is found to be almost constant initially and then starts to decrease when the temperature approaches the glass transition temperature of the bonding adhesive; the interfacial brittleness index B exhibits a similar trend. The proposed temperature-dependent bond-slip model is shown to closely represent the test data upon which it is based, despite the large scatter of the test data.

CE Database subject headings: Fiber reinforced polymer; Concrete; Interface; Bond-slip model; Elevated temperature; Fracture energy.

Introduction

The wide use of externally bonded fiber reinforced polymer (FRP) laminates (including wet layup FRP sheets and pultrued FRP plates) in the strengthening of existing reinforced concrete (RC) structures has been a major development in structural engineering over the past two decades. The success of the FRP strengthening technology has been due to advantages that arise from the high strength-to-weight ratio and excellent corrosion resistance of FRP composites (Teng et al. 2002; Hollaway and Teng 2008). However, the technology also suffers from one major limitation when employed for indoor applications in buildings: FRP composites have a poor resistance to fire as organic polymers (normally epoxies) used both as the matrix material and the bonding adhesive soften quickly around their glass transition temperature T_g (^{o}C) [generally in the range of 45 ^{o}C to 82 ^{o}C (fib 2001; ACI 2008)]. Furthermore, when exposed to a high heat flux, the resin matrix may ignite, resulting in flame spread and smoke generation. This limitation has been a major obstacle to the wider use of the FRP strengthening technology in buildings.

[1] Assistant Professor (Corresponding author), Department of Civil and Structural Engineering, The Hong Kong Polytechnic University, Hong Kong, China. Tel: (852) 2766 6026; Fax: (852) 2334 6389; E-mail: cejgdai@polyu.edu.hk.
[2] PhD Candidate, Department of Civil and Structural Engineering, The Hong Kong Polytechnic University, Hong Kong, China. E-mail: gaowanyang20022003@yahoo.com.cn.
[3] Chair Professor of Structural Engineering, Department of Civil and Structural Engineering, The Hong Kong Polytechnic University, Hong Kong, China. E-mail: cejgteng@polyu.edu.hk.

1

The above-mentioned fire-resistance problem of FRP-strengthened RC structures may be solved by covering the bonded FRP system with a fire protection layer so that the temperature in the FRP stays below its glass transition temperature for a sufficiently long period during a fire (Bisby et al. 2005; Williams et al. 2008); the structural resistance of such a fire-protected FRP-strengthened RC structure will remain basically unaffected during this time period. However, existing studies (e.g. Gamage et al. 2006; Gao et al. 2010) have shown that this approach is usually impractical because the fire protection layer needed can be excessively thick (e.g. 70mm for achieving a two-hour fire resistance rating for the epoxy). As a result, the attractiveness of the FRP strengthening technology in terms of its minimal alterations to the dimensions and appearance of the structure is greatly compromised. In addition, this solution may not be cost-effective.

A more practical solution is to adopt a relatively thin fire protection layer to achieve only partial insulation for the bonded FRP system; such an insulation layer is aimed at preventing flame spread and smoke generation, and in the meantime, ensuring that an adequate structural resistance is retained during a fire. Depending on the situation, the latter requirement may mean that the contribution of the bonded FRP system is allowed to totally disappear, but the structural resistance of the original RC structure is completely or largely preserved after exposure to a fire; it may also mean that the resistance offered by the bonded FRP system is only partially lost during a fire (e.g. due to the deterioration of the bondline).

To be able to explore the benefits of different fire protection strategies and to develop corresponding design procedures, an analysis capability for predicting the behavior of FRP-strengthened RC structures with fire protection of various levels needs to be established. For the development of such an analysis capability, a key component is a bond-slip model for FRP-to-concrete interfaces at elevated temperature. Indeed, as the bond capacity between FRP and concrete may degrade faster than the FRP system itself during a fire (Ahmed and Kodur 2011), the partial loss of the structural resistance offered by the bonded FRP system may be due directly to degradation in bond performance. In addition to fire exposure, FRP-strengthened RC structures are also found in harsh service environments, where temperatures up to 50 $^{\circ}$C or more may occur (e.g. hot climates and industrial conditions). For such service conditions, it is also essential for designers to understand how FRP-to-concrete interfaces behave at elevated temperature and consequently how their degradation influences the safety of FRP-strengthened RC structures. This paper therefore presents a study aimed at the development of the first ever bond-slip model for FRP-to-concrete interfaces at elevated temperature.

Existing experimental studies

Only a few experimental studies have investigated how elevated temperatures influence the bond behavior between the bonded FRP laminate and the concrete substrate. Blontrock (2003) presented the first experimental study in which double-lap shear tests on carbon FRP (CFRP)-to-concrete bonded joints were conducted at four different temperatures (i.e. 20, 40, 55 and 70 $^{\circ}$C). The ultimate load of the FRP-to-concrete bonded joint was found in this study to increase by 41% and 24% when the temperature was increased from 20 $^{\circ}$C to 40 $^{\circ}$C and 55 $^{\circ}$C, respectively. However, when the temperature was further increased to 70 $^{\circ}$C, the ultimate load decreased by 19%.

Similar double-lap shear tests were carried out by Wu et al. (2005) on concrete specimens bonded with carbon fabric sheets. The wet lay-up FRP laminates were formed in two steps: a primer layer was first applied to the concrete surface, followed by the

impregnation and placement of the fabric sheets with an epoxy resin. In one set of the specimens, an ordinary epoxy primer and an ordinary epoxy resin were used; in the other set, their thermo-resistant variants were used. The former specimens were tested at four different temperatures (i.e. 26, 30, 40 and 50 $^{\circ}$C), while the latter were tested at 26, 40, 50 and 60 $^{\circ}$C. For both types of primers and resins, the tests showed that the ultimate load decreased gradually as the temperature increased.

Klamer (2006, 2009) investigated the effect of temperature variation on the debonding behavior of CFRP-to-concrete interfaces using two different test set-ups: double-lap shear tests and small-scale three-point bending tests. Double-lap shear tests were conducted at eight different temperatures (-20, 20, 40, 50, 70, 80, 90 and 100 $^{\circ}$C). The test results showed that the ultimate load increased initially as the temperature increased until it was around the glass transition temperature $T_{g,a}$ of the bonding adhesive which was 62 $^{\circ}$C (Klamer 2006). After that, a further temperature increase resulted in a decrease in the ultimate load due to the softening of the adhesive. The tests also indicated that debonding in the specimens was due to cohesion failure in the concrete adjacent to the adhesive layer at low to moderate temperatures (-20 $^{\circ}$C to 50 $^{\circ}$C), but at elevated temperatures (70 $^{\circ}$C to 100 $^{\circ}$C), debonding was due to adhesion failure at the adhesive-to-concrete interface. A similar trend for ultimate loads was also observed for the three-point bending tests: the ultimate load first increased with the temperature and then decreased with further temperature increases. Klamer et al. (2008) also tested four full-scale FRP-strengthened RC beams at each of three different temperatures (i.e. 20, 50 and 70 $^{\circ}$C) to investigate the effect of temperature variation on the debonding mechanism. These tests showed that the average ultimate load and the failure mode at 50 $^{\circ}$C were similar to those observed at ambient temperature (20 $^{\circ}$C). However, at 70 $^{\circ}$C, the specimens failed by adhesion failure at the adhesive-to-concrete interface, and the average ultimate load reduced considerably. Klamer et al. (2008) suggested that the strength contribution of the FRP strengthening system should be ignored once the temperature at the FRP-to-concrete interface reaches $T_{g,a}$.

Cai (2008) studied the bond behavior between CFRP sheets and concrete at temperatures ranging from 4 $^{\circ}$C to 180 $^{\circ}$C. An increase was seen in the average ultimate load by about 35% for specimens tested at 40 $^{\circ}$C over specimens tested at ambient temperature (i.e. 4 $^{\circ}$C). A further increase in temperature to 100 $^{\circ}$C resulted in a 66% decrease in the average ultimate load. For temperatures exceeding 100 $^{\circ}$C, the ultimate load showed no further decrease as the temperature increased; that is, the ultimate load remained almost unchanged.

Leone et al. (2009) investigated the effect of service temperature (i.e. 20, 50, 65 and 80 $^{\circ}$C) on the bond behavior of FRP-to-concrete bonded joints. Three types of FRP reinforcement including wet lay-up CFRP and Glass FRP (GFRP) sheets as well as pultruded CFRP plates were used in the tests. In the case of CFRP sheets, a temperature increase in the range below $T_{g,a}$ resulted in an increase in the ultimate load while at temperatures beyond $T_{g,a}$, the ultimate load decreased as the temperature increased. The GFRP sheet-to-concrete bonded joints were tested only at 20 $^{\circ}$C and 80 $^{\circ}$C, showing a significant loss of the ultimate load at 80 $^{\circ}$C. However, a different trend was observed for the CFRP plate-to-concrete bonded joints as the ultimate load at 50 $^{\circ}$C was found to be lower than those at 20 $^{\circ}$C and 80 $^{\circ}$C, probably due to the insufficient penetration of the bonding adhesive into the concrete in some areas as reported by Leone et al. (2009).

The existing laboratory tests as reviewed above have demonstrated clearly that elevated temperatures (or more generally temperature variations) have a significant effect on the bond behavior of FRP-to-concrete interfaces. In most of these existing studies, the ultimate load of the bonded joint was found to increase before the temperature reached the glass transition temperature. This was due to the effect of initial thermal stresses induced along the FRP-to-concrete interface as explained by Gao et al. (2012). The decrease of the ultimate load

3

afterwards was due to degradations in the interfacial bond, which can be described using a degraded bond-slip model. In the development of a bond-slip model for such degraded interfaces based on bonded joint tests at elevated temperature, the effect of thermal stresses needs to be isolated and excluded in interpreting the test results.

Formulation of the bond-slip model

General

There are basically three different ways of developing a bond-slip model for FRP-to-concrete interfaces: (a) based directly on readings from closely-spaced strain gauges installed on the surface of the FRP laminate (e.g. Chajes et al. 1996; Nakaba et al. 2001; Bilotta et al. 2012); (b) based on detailed meso-scale finite element modeling of debonding failures in conjunction with test data (e.g. distributions of strains in the FRP laminate along the bond length) (Lu et al. 2005a); (c) based on the global load-displacement responses of FRP-to-concrete bonded joints (Dai et al. 2005). Method (a) suffers from a number of problems and has not been used successfully for this purpose; in particular, the test data show considerable scatter due to factors such as the local bending of the FRP laminate and heterogeneity of the concrete substrate due to non-uniform aggregate and crack distributions. Method (b) is based on rigorous numerical modeling and has led to the well-known bond-slip model of Lu et al. (2005b). Method (a) was not employed in the present study due to not only the scatter problem but also the lack of sufficient strain measurement data. Method (b) was also not attempted in the present study due to a lack of understanding of detailed local material degradations of FRP-to-concrete interfaces at elevated temperature; the modeling of adhesion failure at the adhesive-concrete interface poses a particular challenge to this approach. Therefore, Method (c) was adopted, and indeed the proposed model represents an extension of the two-parameter bond-slip model developed by Dai et al. (2005) for FRP-to-concrete interfaces at ambient temperature.

The advantage of Dai et al.'s approach lies in its simplicity as only two parameters need to be determined from test data without the need for sophisticated finite element modeling. Another justification for using Dai et al.'s approach in the present study is that the softening of adhesives at elevated temperature can be implicitly reflected in these two parameters. Although the use of two parameters only to define the bond-slip law may impose some unnecessary constraint in achieving an accurate description of the shape of highly non-linear bond-slip curves, the extension of Dai et. al. (2005) model for the present purpose represents a good first attempt within the context of available information for FRP-to-concrete interfaces exposed to elevated temperatures.

Theoretical background

The single-lap or double-lap shear test is a popular method for studying the bond characteristics of FRP-to-concrete interfaces (Fig. 1). In deriving local bond-slip curves using Dai et al.'s (2005) approach, load-displacement responses from such tests are interpreted in accordance with the theoretical framework presented below.

Bond-slip model

At any location of the FRP-to-concrete interface of an FRP-to-concrete bonded joint with the free end of the FRP laminate subjected to a pull load, the relationship between the axial strain in the FRP and the interfacial slip between the FRP and the concrete can be expressed

as follows:

$$\varepsilon(x) = f(\delta(x)) \tag{1}$$

By assuming that the $\tau \sim \delta$ relationship is unique along the FRP-to-concrete interface, Eq. 1 is valid for all locations of a sufficiently long bond length (Dai et al. 2005, 2006). Therefore, Eq. 1 can be simply obtained from the pull load (from which the strain in the FRP at the loaded end can be found) and the relative interfacial slip between the FRP and the concrete at the loaded end. It should be noted that, when the FRP-to-concrete interface is subjected to combined mechanical and thermal loadings, the strain in the FRP at the loaded end consists of both the load-induced and the thermally induced components as shown later.

From an interpretation of extensive experimental results of bonded joints tested at ambient temperature, the following exponential expression was found to represent $f(\delta(x))$ with sufficient accuracy (Dai et al. 2005):

$$\varepsilon(x) = f(\delta(x)) = A(1 - e^{-B \cdot \delta(x)}) \tag{2}$$

where A and B are parameters to be determined from regression analysis of bonded joint test results. The physical meaning of A is the maximum strain reached in the FRP laminate if its bond length is longer than the effective bond length. B can be regarded as the brittleness index that controls the shape of the bond-slip curve: a larger B value corresponds to a steeper ascending branch (i.e. a larger initial interfacial stiffness) and a steeper descending branch.

Note that

$$\tau(x) = \frac{E_p t_p}{(1+\alpha)} \frac{d\varepsilon(x)}{dx} \tag{3}$$

and

$$\varepsilon(x) = \frac{d\delta(x)}{dx} \tag{4}$$

where $\frac{E_p t_p}{(1+\alpha)}$ is a stiffness ratio of the bonded joint with $\alpha = \frac{E_p t_p b_p}{E_c t_c b_c}$; b_p and t_p are the width and thickness of the FRP laminate; b_c and t_c are the width and thickness of the concrete prism; E_p and E_c are the elastic moduli of the FRP laminate and the concrete, respectively.

Combining Eqs. 2-4 yields the following equation for the bond-slip model of FRP-to-concrete interfaces:

$$\tau(x) = A^2 B \frac{E_p t_p}{(1+\alpha)} (e^{-B\delta(x)} - e^{-2B\delta(x)}) \tag{5}$$

If G_f is used to denote the interfacial fracture energy, which is the area underneath the $\tau \sim \delta$ curve (i.e. $\int_0^\infty \tau(x)d\delta(x) = G_f$), the following expression can be obtained from Eq. 5:

$$A = \sqrt{\frac{2G_f}{E_p t_p}(1 + \alpha)} \tag{6}$$

By substitution of Eq. 6 into Eq. 5, the bond-slip model can be rewritten as

$$\tau(x) = 2G_f B\left(e^{-B\delta(x)} - e^{-2B\delta(x)}\right) \tag{7}$$

Interfacial slip distribution

Using Eqs. 3-5, the governing differential equation for the FRP-to-concrete interface subjected to shear stresses can also be expressed in terms of the local interfacial slip $\delta(x)$ as follows:

$$\frac{\mathrm{d}^2\delta(x)}{\mathrm{d}x^2} = A^2 B\left(e^{-B\delta(x)} - e^{-2B\delta(x)}\right) \tag{8}$$

For an FRP-to-concrete interface with a sufficiently long bond length and subjected to combined thermal and mechanical loadings, the solution to Eq. 8 can be found without difficulty following the procedure described in Dai et al. (2006):

$$\delta(x) = \frac{1}{B}\ln\left[e^{B(Ax+c_2)} + 1\right] \tag{9}$$

where c_2 is a constant given by the following equation:

$$c_2 = \frac{1}{B}\ln\left\{\frac{\frac{1}{A}\left[\frac{P(1+\alpha)}{E_p t_p b_p} + (\alpha_p - \alpha_c)\Delta T\right]}{1 - \frac{1}{A}\left[\frac{P(1+\alpha)}{E_p t_p b_p} + (\alpha_p - \alpha_c)\Delta T\right]}\right\} - AL \tag{10}$$

where P is the pull load acting on the FRP laminate at the loaded end; L is the bond length; and ΔT is the temperature variation (a positive value means a temperature increase).

It should be mentioned that viscoelastic deformation of FRP-to-concrete interfaces is not considered in the proposed model, while such deformation may become significant at elevated temperatures when the interface is subjected to sustained loading. In all existing shear tests on FRP-to-concrete joints at elevated temperatures, the specimen was usually first heated up to the desired temperature and was then subjected to instantaneous loading to failure. The interfacial stresses induced by the thermal mismatch between FRP and concrete are generally highly localized and relatively low, so they are also not expected to induce significant viscoelastic deformation.

Ultimate pull load

Considering the differential thermal expansion between FRP and concrete, at any location of the interface, the pull load $P(x)$ acting on the FRP laminate can be calculated as

$$P(x) = \frac{E_p t_p b_p}{(1+\alpha)}\left[\varepsilon(x) - (\alpha_p - \alpha_c)\Delta T\right] \tag{11}$$

Substituting Eq. 2 into Eq. 11, the pull load-displacement relationship (i.e. P-Δ relationship) at the loaded end can be obtained as

$$P = \frac{E_p t_p b_p}{(1+\alpha)}\left[A(1 - e^{-B\Delta}) - (\alpha_p - \alpha_c)\Delta T\right] \tag{12}$$

If the second term on the right hand side is removed, Eq. 12 is identical to the pull load-slip relationship derived by Dai et al. (2005) for FRP-to-concrete interfaces at ambient temperature.

If there is an infinite bond length (e.g. at least a bond length longer than the effective bond length) to provide a large enough slip Δ at the loaded end, Eq. 12 converges to the following form:

$$P_{uT} = b_p \sqrt{2G_f \frac{E_p t_p}{(1+\alpha)}} - \frac{E_p t_p b_p}{(1+\alpha)}(\alpha_p - \alpha_c)\Delta T \tag{13}$$

where P_{uT} is the ultimate pull load of the FRP-to-concrete interface subject to combined mechanical and thermal loadings. When $\Delta T = 0$, Eq. 13 reduces to the familiar relationship between the ultimate pull load and the interfacial fracture energy of an FRP-to-concrete interface at ambient temperature (e.g. Taljsten 1996; Brosens 2001; Wu et al. 2002; Yuan et al. 2004).

Strain distributions in the FRP laminate

Since $\delta(x)$ is known, with the use of Eqs. 6, 9, 10 and 13, the strain distribution, $\varepsilon(x)$, in the FRP laminate along the FRP-to-concrete interface at different pull load levels can also be obtained as

$$\varepsilon(x) = \frac{A}{1+e^{BA(L-x)} \cdot \dfrac{P_{uT}-P}{P+\frac{E_p t_p b_p}{(1+\alpha)}(\alpha_p-\alpha_c)\Delta T}} \tag{14}$$

Determination of G_f and B

With the above theoretical framework, the values of the two key parameters, G_f and B, for the bond-slip model, can be determined from the pull test result without difficulty for a given FRP-to-concrete interface subjected to combined mechanical and thermal loadings. For a single-lap shear test or one of the four interfaces in a double-lap shear test (the latter has been widely used to evaluate the bond behavior of FRP-to-concrete interfaces at elevated temperature as reviewed earlier), the interfacial facture energy G_f can be calculated from the ultimate pull load and Eq. 13 as follows provided that the bond length is longer than the effective bond length:

$$G_f(T) = (1 + \alpha)\frac{(P_{uT}-\Delta P)^2}{2E_p t_p b_p^2} \tag{15}$$

where $\Delta P = -\frac{E_p t_p b_p}{(1+\alpha)}(\alpha_p - \alpha_c)\Delta T$, which is induced by the thermal incompatibility between FRP and concrete. It is seen that the difference in thermal expansion between FRP and concrete has a positive influence on the ultimate load when the bonded joint is exposed to a moderate temperature increase and vice versa provided no material degradation of the bondline has occurred. Therefore, when deducing the temperature-dependent fracture energy from the pull load, the thermal stress-induced component ΔP needs to be eliminated first.

It should also be noted that the elastic modulus E_p of the FRP laminate in Eq. 15 may change with the temperature increase. Bisby (2003) collected existing test data and proposed a sigmoid function model for the strength and elastic modulus degradation of pre-fabricated FRP products at elevated temperature. However, Bisby's model may not be suitable for wet layup FRP sheets as they possess a much lower T_g than prefabricated FRP products. For wet layup FRP sheets, the matrix and the bonding materials are generally the same epoxy material

7

which cannot be completely cured at ambient temperature (Silva and Biscaia 2008), and its T_g is normally within the range of 45 $^{\circ}$C to 82 $^{\circ}$C (fib 2001; ACI 2008). By contrast, the polymer matrix in a prefabricated FRP composite has a much higher T_g [around 130 $^{\circ}$C (Clarke 1996)] as prefabrication allows curing at elevated temperature and pressure (Stratford et al. 2009).

Unfortunately, previous researchers did not provide details of the temperature-dependent properties (e.g. elastic modulus) of FRP laminates when reporting their test results of FRP-to-concrete bonded joints at elevated temperatures, which made it difficult to interpret the joint test results. To tackle this problem, the authors collected the available test data of the elastic modulus of FRP sheets at elevated temperatures from other published studies (Chowdhury et al. 2008; Chowdhury et al. 2011). It was assumed that all FRP sheets have a similar degradation trend at elevated temperatures and the actual degradation process depends on the glass transition temperature $T_{g,p}$. Fig. 2a shows the available test data for the elastic modulus of FRP sheets at elevated temperature. The test data from Zhou (2005) and Wang et al. (2007) for FRP bars and the two models proposed by Bisby (2003) for CFRP and GFRP respectively are also shown there for comparison. In the figure, the elastic modulus at elevated temperature is normalized by the corresponding value obtained at ambient temperature. It is clearly seen that the elastic modulus degradation of FRP sheets is more severe than that of FRP bars. As the performance of FRP sheets/bars at elevated temperature depends predominately on the glass transition temperature $T_{g,p}$ of the polymer matrix, $T_{g,p}$ needs to be taken as a key parameter in any elastic modulus degradation model. Therefore, Bisby's (2003) model was modified, by taking account of the $T_{g,p}$ value ($^{\circ}$C), into the following equation to describe the elastic modulus degradation of FRP sheets:

$$\frac{E_{pT}}{E_{p0}} = \left(\frac{1-a_1}{2}\right) \times \tanh\left(-a_2 \times \left(\frac{T}{T_{g,p}} - a_3\right)\right) + \left(\frac{1+a_1}{2}\right) \tag{16}$$

where E_{p0} and E_{pT} are the elastic modulus of FRP at ambient temperature and that at an elevated temperature T ($^{\circ}$C), respectively; and $a_1 = 0.729$, $a_2 = 9.856$ and $a_3 = 0.607$ are empirical factors derived based on multivariable least-squares regression analysis of existing test data. Fig. 2b shows this proposed relationship where the elastic modulus is normalized by its corresponding ambient value and the temperature is normalized by the $T_{g,p}$ value ($^{\circ}$C) of the polymer matrix. The highest test temperature covered by Fig. 2b is 200 $^{\circ}$C. While this temperature is still much lower than the decomposition temperature of polymer matrix [denoted by T_d, around 400 $^{\circ}$C (Mouritz and Gibson 2006)], the proposed model is adequate for bond critical applications as the FRP-to-concrete interface has lost most of its bond capacity around this temperature. For contact critical applications (e.g. FRP-confined columns), further work is needed to define the stiffness degradation of FRP sheets beyond 200°C for accurate predictions of member residual strengths at higher temperatures. Due to the lack of test data for $T_{g,p}$ as well as the elastic modulus of FRP plates at elevated temperature (Wang et al. 2011), the original Bisby's (2003) model developed for FRP bars is directly used in the present study to predict the elastic modulus of FRP plates at elevated temperature.

Once the value of G_f (i.e. A) is known (Eq. 15), the value of B can be obtained from least-squares regression analysis of the experimental relationship between the pull load and the local slip at the loaded end. Unfortunately, of the existing experimental studies, only Klamer (2006) reported the global pull load-displacement curves of FRP-to-concrete bonded joints at elevated temperature. Such relationships were not reported for the tests conducted by other researchers. Instead, the strain distributions over the FRP laminate at different pull load

levels were often reported. As the measured strains in the FRP include various local effects (e.g. local bending of the FRP laminate and non-uniform distributions of coarse aggregate and cracks in the substrate concrete), the global load-displacement curve, if available, was used in determining the value of B from each joint test. If this was not available, Eq. 14, which represents the theoretical strain distribution in the FRP, was compared with the test strain distribution to determine the value of B.

If the measured strains at different pull load levels (P_i, $i = 1, \dots m$) and at different locations ($j = 1, \dots n$, where n is the total number of strain gages on the FRP laminate) are denoted by $(\varepsilon_{i,j})^{\text{test}}$ and the corresponding strains predicted by Eq. 14 are denoted by $(\varepsilon_{i,j})^{\text{pred}}$, the value of B can be determined through least square minimization of the difference between $(\varepsilon_{i,j})^{\text{test}}$ and $(\varepsilon_{i,j})^{\text{pred}}$. That is, for each bonded joint test, a value for B can be found to minimize (Dai and Ueda 2003):

$$\text{e} = \sum_{i=1}^{m}\sum_{j=1}^{n}\left[(\varepsilon_{i,j})^{\text{pred}} - (\varepsilon_{i,j})^{\text{test}}\right]^2 \tag{17}$$

When the global pull load-displacement curve was used to obtain the value of B for test joint, a similar procedure was followed.

It should be noted that in most existing tests of FRP-to-concrete bonded joints at elevated temperature, strain readings were not taken during the heating process; that is, the reported strain readings did not include the initial strains in the FRP laminate induced by thermal incompatibility between FRP and concrete (Blontrock 2003; Wu et al. 2005; Leone et al. 2009). Therefore, when such data are used in regression analysis, the initial thermal strains need also be eliminated from the predicted strains.

Expressions for G_f and B

The test data of 79 bonded joint shear tests conducted at ambient and elevated temperatures were assembled from the existing experimental studies reviewed earlier (Blontrock 2003; Klamer 2006; Wu et al. 2005; Cai 2008; Leone et al. 2009) to examine the dependence of G_f and B on temperature following the approach explained above. All these test results were from double-lap shear tests with a sufficient FRP bond length. Details of all the specimens and their test results are shown in Table 1. In the tests of Cai (2008) and Lenoe et al. (2009), the T_g values (including both $T_{g,a}$ and $T_{g,p}$) were determined by the researchers using the differential scanning calorimetry (DSC) method, while in the tests of Blontrock (2003), Wu et al. (2005) and Klamer (2006), the T_g values were provided by the material suppliers. In the case of FRP sheets, as the bonding adhesive is also used as the polymer matrix, the values of $T_{g,a}$ and $T_{g,p}$ are usually identical. Only Wu et al. (2008) used two different thermo-resistant resins as the bonding adhesive and the polymer matrix of the FRP sheets respectively, and hence the values of $T_{g,a}$ and $T_{g,p}$ for their tests are different.

A summary of the predicted values for ΔP, G_f, A and B are given in Table 2. Specimens C-L-20 to C-L-80 in Leone et al.'s (2009) tests were not included in the analysis since they suffered from insufficient penetration of the bonding adhesive into the concrete substrate as reported by the authors. Specimens B1-100 and B2-70 from Klamer (2006) were excluded in the determination of B because of suspected measurement errors: the global pull force was recorded to increase abruptly with almost zero slip at the loaded end in the initial loading stage. Through a careful analysis of the test data, the following observations can be made:
(1)   When the temperature increases from ambient temperature but remains below the glass

9

transition temperature of the bonding adhesive ($T_{g,a}$), the interfacial facture energy G_f of the FRP-to-concrete interface remains almost constant (Fig. 3). For the few specimens tested by Blontrock (2003), Leone et al. (2009) and Cai (2008), an initial increase in the interfacial fracture energy is also observed. Post-curing at elevated temperature (Klamer 2006) is believed to be the main reason for this phenomenon. During this stage, no degradation of the interface occurred.

(2)　As the temperature increases further, the interfacial fracture energy G_f is initially almost constant but starts to decrease when the glass transition temperature is being approached; a rapid decrease is seen to occur when the temperature exceeds the glass transition temperature of the bonding adhesive (Fig. 3). This decrease is mainly attributed to the mechanical degradation of the bonding adhesive.

(3)　The value of B also shows a decreasing trend as the temperature increases (Fig. 4), but this decrease is almost completed when the glass transition temperature is reached, which is different from that observed for the interfacial fracture energy. A decrease in the B value means a decrease in the interfacial stiffness due to the softening of the bonding adhesive (Dai et al. 2005).

As the properties of a bonding adhesive at elevated temperature relies highly on its glass transition temperature, the value of $T_{g,a}$ (°C) needs to be properly accounted for in establishing mathematical expressions for G_f and B. Figs. 3 and 4 show how the values of G_f and B normalized by their ambient values vary with the value of temperature normalized by $T_{g,a}$(°C). Through multivariable least-squares regression analysis, the following two expressions for Eq. 7 can be derived to completely define a temperature-dependent bond-slip model:

$$\frac{G_f(T)}{G_{f0}} = \frac{1}{2} \times \tanh\left(-b_2 \times \left(\frac{T}{T_{g,a}} - b_3\right)\right) + \frac{1}{2} \tag{18}$$

$$\frac{B(T)}{B_0} = \frac{(1-c_1)}{2} \times \tanh\left(-c_2 \times \left(\frac{T}{T_{g,a}} - c_3\right)\right) + \frac{(1+c_1)}{2} \tag{19}$$

where B_0 (mm^{-1}) and G_{f0} (N/mm) are respectively the interfacial brittleness index and the interfacial fracture energy at ambient temperature; and b_2= 3.206, b_3= 1.313, c_1= 0.485, c_2= 14.053 and c_3= 0.877. Eqs. 18 and 19 approximate the test results reasonably well given the larger scatter of the test data (Figs 3 and 4). The average of the predicted-to-test fracture energy ratios and its coefficient of variation are 1.025 and 32.857%, while the average of the predicted-to-test brittleness index ratios and its coefficient of variation are 1.084 and 20.163%. The values of B_0 and G_{f0} may vary over a wide range and depend mainly on the strength of concrete and the properties of adhesive (Dai et al. 2005; Lu et al. 2005b; Bilotta et al. 2011; Toutanji et al. 2011). A joint shear test should be conducted to determine the values of these two parameters for a specific type of FRP laminate (and adhesive). If such a test cannot be conducted for whatever reason, the interfacial fracture energy G_{f0} can be estimated from Lu et al.'s (2005b) model; for example, Lu et al.'s (2005b) model predicts a value of 0.545 N/mm for G_{f0} for a concrete cylinder compressive strength of 35 MPa and a commonly available bonding adhesive. B_0 may also be determined from Lu et al's (2005b) model; the values of B_0 predicted by Lu et al.'s (2005b) model range from around 8 to around 14.1 for normal strength concrete with a cylinder strength varying from around 15MPa to around 50MPa. Therefore, for simplicity, a simple reference value of 10.4 may be used for B_0 according to Dai et al. (2006) if a conventional bonding adhesive is used.

Predictions from the proposed bond-slip model (Eqs 7, 18 and 19) at various temperatures are presented in Figs. 5a and 5b for Blontrock's (2003) specimens (specimens Zijde-20 to Zijde-70) and some of Klamer's (2006) specimens (specimens B1-20 to B1-100), respectively. The values of G_{f0} and B_0 for Klamer's (2006) specimens were averaged from the two identical specimens tested at ambient temperature. It is clearly seen that as the temperature increases, the initial stiffness of the bond-slip curve decreases while the descending branch becomes more gentle. The area enclosed by the bond-slip curve shrinks as the temperature increases, indicating degradations in the interfacial fracture energy.

Validation of the Bond-Slip Model

Ultimate loads of double-lap shear tests

Fig. 6a presents a comparison between the ultimate load $P_{uT,\text{pred}}$ predicted using the proposed bond-slip model and the test ultimate load $P_{uT,\text{test}}$. The average of the predicted-to-test load ratios and its coefficient of variation are 1.01 and 20.23%, respectively. This comparison indicates that the proposed bond-slip model can be used to predict the ultimate load of a bonded joint at elevated temperature with good accuracy. While this close agreement can be expected because the interfacial fracture energy G_f, upon which the ultimate load depends directly, was regressed from the test ultimate loads, it at least demonstrates that the complex relationships among G_f, the temperature of the FRP-to-concrete interface and the glass transition temperature of the bonding adhesive have all been well captured by Eq. 18. Fig. 6b shows the dependence of the predicted-to-test load ratio on the temperature of the interface. It is seen that the debonding load is reasonably well predicted at temperatures over a wide range (up to 180 °C).

Strain distributions in the FRP laminate

With the proposed bond-slip model, Eq. 14 can be used to predict strain distributions along the FRP laminate at various load levels. In Figs. 7a-7d, predicted strain distributions are compared with experimental strain distributions for four bonded joints at different load levels and different temperatures. The first specimen (Zijde-20) was tested by Blontrock (2003) at ambient temperature (Fig. 7a) while the second specimen (Zijde-55) was tested by Blontrock (2003) at the elevated temperature of 55 °C (Fig. 7b). The bond lengths of both specimens are 300 mm, which is longer than the effective bond length. The predicted strain distributions shown in Fig. 7a were obtained from Eq. 14 with B_0 = 10.29 mm^{-1}, which was regressed from the corresponding experimental FRP strain distributions. In Fig. 7b, two sets of predicted FRP strain distributions are provided. One was predicted using Eq. 14 and B = 5.97 mm^{-1}, which was regressed from the experimental strain distributions; another was predicted using Eq. 14 and B = 7.25 mm^{-1}, which was calculated from the proposed equation for B (Eq. 19). It is seen that both sets of predictions are in close agreement with the test results. By comparing the strain distributions between specimen Zijde-20 and specimen Zijde-55, it can be seen that due to the temperature increase, the strain distributions become more gentle due to the softening of the bonding adhesive. Similar comparisons of strain distributions are shown in Figs. 7c and 7d for the specimens tested by Leone et al. (2009) at ambient temperature (G-S-20, 20 °C) and at an elevated temperature (G-S-80, 80 °C) respectively. Once again, the predicted strain distributions are in close agreement with the measured distributions throughout the loading process. The above comparisons clearly demonstrate the validity of the proposed bond-slip model at least within the parameter ranges of the assembled

test database.

Conclusions

A general approach has been presented to interpret and model the bond-slip behavior of FRP-to-concrete interfaces at elevated temperature. Based on a careful analysis of the existing test data which includes 79 tests of FRP-to-concrete bonded joints at temperatures ranging from 4 ^{o}C to 180 ^{o}C, a nonlinear temperature-dependent local bond-slip model for FRP-to-concrete interfaces has been formulated. This model is an extension of the two-parameter bond-slip model previously proposed by Dai et al. (2005) for FRP-to-concrete interfaces at ambient temperature. The two key parameters employed in the bond-slip model, the interfacial fracture energy G_f (i.e. the area beneath the bond-slip curve) and the interfacial brittleness index B (a shape parameter for the bond-slip curve), were determined from regression analysis of existing test data at elevated temperature. During the interpretation of the test data and the derivation of G_f and B, the influences of both temperature-induced thermal stress and temperature-induced bond degradation were carefully considered. It has been shown that the interfacial fracture energy G_f is initially almost constant but starts to decrease as the temperature approaches the glass transition temperature; the interfacial brittleness index B also exhibits a decreasing trend, but the decrease is almost completed before reaching the glass transition temperature. The proposed temperature-dependent bond-slip model has been shown to provide a reasonably close representation of the test data upon which it is based, despite the large scatter of the test data. The proposed bond-slip model is expected to be useful in the theoretical modeling of FRP-strengthened RC members exposed to fire or extremely hot climates.

Acknowledgements

References

American Concrete Institute (ACI). (2008). "Guide for the design and construction of externally bonded FRP systems for strengthening concrete structures." *ACI 440.2R-08*, Farmington Hills, Michigan, America.

Ahmed, A., and Kodur, V.K.R. (2011). "Effect of bond degradation on fire resistance of FRP-strengthened reinforced concrete beams." *Composites Part B: Engineering*, Vol. 42, No. 2, pp. 226-237.

Bilotta, A., Faella, C., Martinelli, E., and Nigro, E. (2012). "Indirect identification method of bilinear interface laws for FRP bonded on a concrete substrate." *Journal of Composites for Construction*, ASCE, Vol. 16, No. 2, pp. 171-184.

Bisby, L. (2003). "Fire behavior of fiber-reinforced polymer (FRP) reinforced or confined concrete." Ph. D. thesis, Queen's University, Kingston, Ontario, Canada.

Bisby, L.A., Kodur, V.K.R., and Green, M.F. (2005). "Fire endurance of fiber-reinforced polymer-confined concrete columns." *ACI Structural Journal*, Vol. 102, No. 6, pp. 883-891.

Blontrock, H. (2003). "Analysis and modeling of the fire resistance of concrete elements with externally

bonded FRP reinforcement." Ph. D. thesis, Ghent University, Ghent, Belgium.

Brosens, K. (2001). "Anchoring of externally bonded steel plates and CFRP laminates for the strengthening of concrete elements." Ph.D. thesis, Department of Civil Engineering, Katholieke University Leuven, Belgium.

Cai, Z.H. (2008). "Research on bond property of FRP-to-concrete interface under elevated temperatures." Master's thesis, Tongji University, Shanghai, China.

Chajes, M.J., Finch, W.W., Januszuka, T.F., and Thomson, T.A. (1996). "Bond and force transfer of composite material plates bonded to concrete." *ACI Structural Journal*, Vol. 93, No. 2, pp. 208-217.

Chowdhury, E.U., Eedson, R., Bisby, L.A., Green, M.F., Benichou, N., and Kodur, V.K.R. (2008). "Mechanical characterization of fibre reinforced polymers for numerical fire endurance modelling." *Proceeding of the Fifth International Conference on Structures in Fire*, Singapore, pp. 499-507.

Chowdhury, E.U., Eedson, R., Green, M.F., Bisby, L.A., and Benichou, N. (2011). "Mechanical characterization of fiber reinforced polymers materials at high temperature." *Fire Technology*, Vol. 47, No. 4, pp. 1063-1080.

Clarke, J.L. (1996). *Structural design of polymer composites – Eurocomp design code and handbook*. E & FN Spon. Ltd., London, UK.

Dai, J.G., and Ueda, T. (2003). "Local bond stress slip relationship for FRP composites-concrete interfaces." *Proceedings of the Sixth International Symposium on FRP Reinforcement for Concrete Structures (FRPRCS-6)*, Singapore, pp. 143-152.

Dai, J.G., Ueda, T., and Sato, Y. (2005). "Development of the nonlinear bond stress-slip model of fiber reinforced plastics sheet-concrete interfaces with a simple method." *Journal of Composites for Construction*, ASCE, Vol. 9, No. 1, pp. 52-62.

Dai, J.G., Ueda, T., and Sato, Y. (2006). "Unified analytical approaches for determining shear bond characteristics of FRP-concrete interfaces through pullout tests." *Journal of Advanced Concrete Technology*, JSCE, Vol. 4, No. 1, pp. 133-145.

Féderation International du Béton (fib). (2001). "Externally bonded FRP reinforcement for RC structures." *fib Bulletin 14*, fib Task Group 9.3, fib, Lausanne, Switzerland.

Gamage, J.C.P.H., Al-Mahaidi, R., and Wong, M.B. (2006). "Bond characteristics of CFRP plated concrete members under elevated temperatures." *Composite Structures*, Vol. 75, No. 1-4, pp. 199-205.

Gao, W.Y., Hu, K.X., and Lu, Z.D. (2010). "Fire resistance experiments of insulated CFRP strengthened reinforced concrete beams." *China Civil Engineering Journal*, Vol. 43, No. 3, pp. 15-23.

Gao, W.Y., Teng, J.G., and Dai, J.G. (2012). "Effect of temperature variation on the full-range behavior of FRP-to-concrete bonded joints." *Journal of Composites for Construction,* ASCE, (in press) doi:10.1061/(ASCE)CC.1943-5614.0000296.

Hollaway, L.C., and Teng, J.G. (2008). *Strengthening and rehabilitation of civil infrastructures using FRP composites*. Woodhead Publishing Limited, Cambridge, UK.

Klamer, E. (2006). "The influence of temperature on concrete structures strengthened with externally bonded CFRP." *Research Report*, Eindhoven University of Technology, Eindhoven, Netherlands.

Klamer, E.L., Hordijk, D.A., and Hermes, M.C.J. (2008). "The influence of temperature on RC beams strengthened with externally bonded CFRP reinforcement." *Heron*, Vol. 53, No. 3, pp. 157-185.

Klamer, E. (2009). "Influence of temperature on concrete beams strengthened in flexure with CFRP." Ph.D. thesis, Eindhoven University of Technology, Eindhoven, Netherlands.

Leone, M., Matthys, S., and Aiello, M.A. (2009). "Effect of elevated service temperature on bond between FRP EBR systems and concrete." *Composites Part B: Engineering*, Vol. 40, No. 1, pp. 85-93.

Lu, X.Z., Ye, L.P., Teng, J.G., and Jiang, J.J. (2005a). "Meso-scale finite element model for FRP sheets/plates bonded to concrete." *Engineering Structures*, Vol. 27, No. 4, pp. 564-575.

Lu, X.Z., Teng, J.G., Ye, L.P., and Jiang, J.J. (2005b). "Bond-slip models for FRP sheets/plates bonded to concrete." *Engineering Structures*, Vol. 27, No. 6, pp. 920-937.

Mouritz, A. P., and Gibson, A. G. (2006). *Fire properties of polymer composite materials*, Springer, Dordrecht, Netherlands.

Nakaba, K., Kanakubo, T., Furuta, T., and Yoshizawa, H. (2001). "Bond behavior between fiber-reinforced polymer laminate and concrete." *ACI Structural Journal*, Vol. 98, No. 3, pp. 359-367.

Silva, M.A.G., and Biscaia, H. (2008). "Degradation of bond between FRP and RC beams." *Composite Structures*, Vol. 85, No. 2, pp. 164-174.

Stratford, T.J., Gillie, M., Chen, J.F., and Usmani, A.S. (2009). "Bonded fibre reinforced polymer strengthening in a real fire." *Advances in Structural Engineering*, Vol. 12, No. 6, pp. 867-878.

Taljsten, B. (1996). "Strengthening of concrete prisms using the plate-bonding technique." *International Journal of Fracture*, Vol. 82, No. 3, pp. 253-266.

Toutanji, H., Han, M., and Ghorbel, E. (2011). "Interfacial bond strength characteristics of FRP and RC substrates." *Journal of Composites for Construction*, ASCE, Vol. 16, No. 1, pp. 35-46.

Teng, J.G., Chen, J.F., Smith, S.T., and Lam, L. (2002). *FRP-strengthened RC structures*. John Wiley and Sons Ltd., Chichester, UK.

Wang, K., Young, B., and Smith, S.T. (2011). "Mechanical properties of pultruded carbon fibre-reinforced polymer (CFRP) plates at elevated temperatures." *Engineering Structures*, Vol. 33, No. 7, pp. 2154-2161.

Wang, Y.C., Wong, P.M.H., and Kodur, V. (2007). "An experimental study of the mechanical properties of fibre reinforced polymer (FRP) and steel reinforcing bars at elevated temperatures." *Composite Structures*, Vol. 80, No. 1, pp. 131-140.

Williams, B., Kodur, V.K.R., Green, M.F., and Bisby, L. (2008). "Fire endurance of fiber-reinforced polymer strengthened concrete T-beams." *ACI Structural Journal*, Vol. 105, No. 1, pp. 60-67.

Wu, Z.S., Iwashita, K., Yagashiro, S., Ishikawa, T., and Hamaguchi, Y. (2005). "Temperature effect on bonding and debonding behavior between FRP sheets and concrete." *Journal of the Society of Materials Science*, Vol. 54, No. 5, pp. 474-480.

Wu, Z.S., Yuan, H., and Niu, H. (2002). "Stress transfer and fracture propagation in different kinds of adhesive joints." *Journal of Engineering Mechanics*, ASCE, Vol. 128, No. 5, pp. 562-573.

Yuan, H., Teng, J.G., Seracino, R., Wu, Z.S., and Yao, J. (2004). "Full-range behavior of FRP-to-concrete bonded joints", *Engineering Structures*, Vol. 26, No. 5, pp. 553-565.

Zhou, C.D. (2005). "Fire performance of GFRP reinforced concrete." Research Report, Department of Civil Engineering, Tongji University, Shanghai, China.

Fig. 1. Schematic of a single-lap shear test.
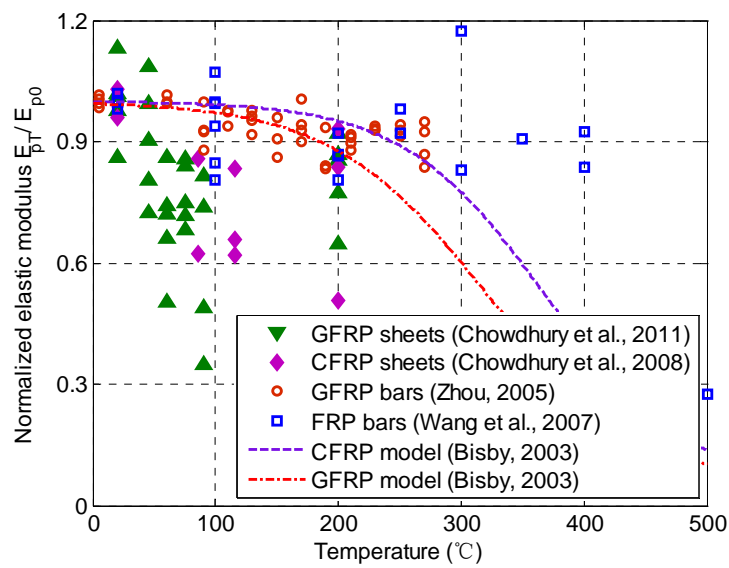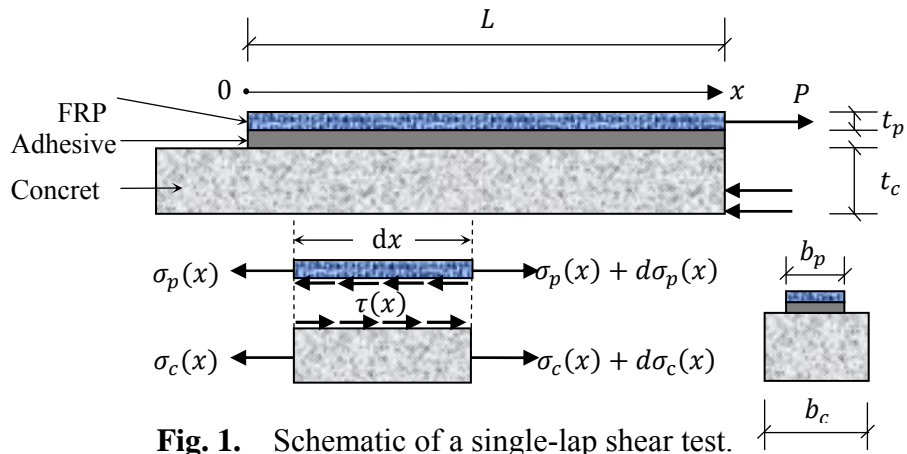
(a) Effect of temperature on normalized elastic modulus
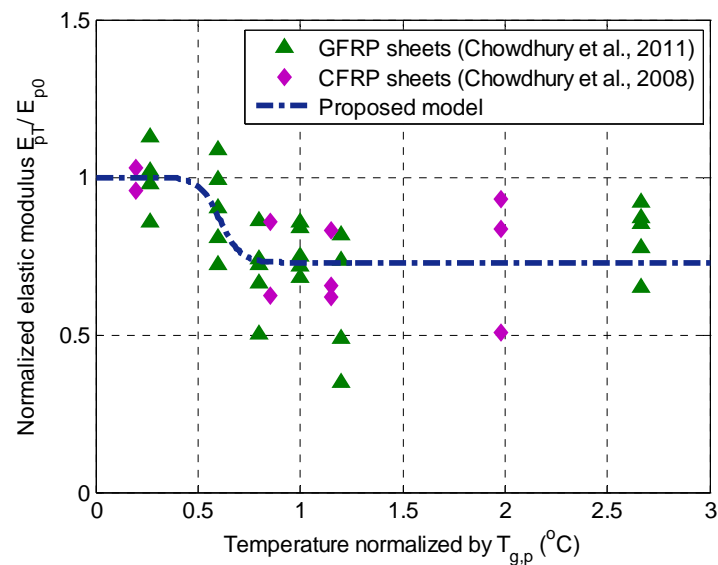
(b) Effect of normalized temperature ($T/T_{g,p}$) on normalized elastic modulus

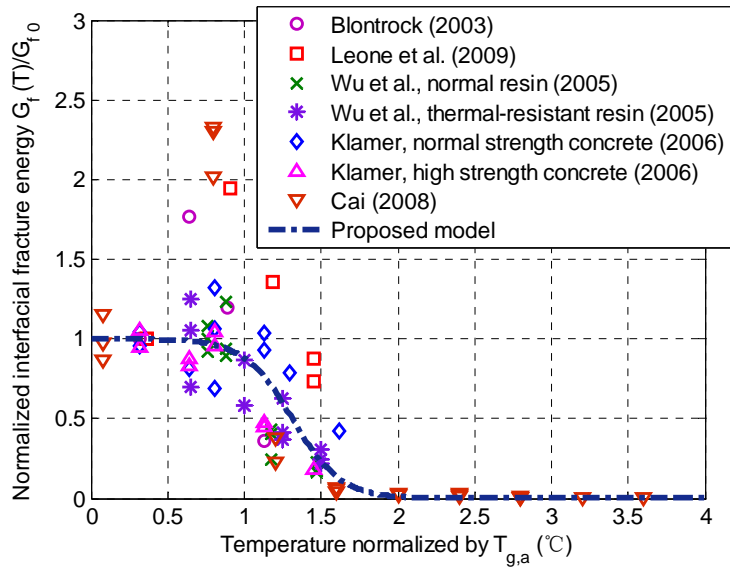**Fig. 2.** Elastic modulus degradations of FRP sheets/bars at elevated temperature.

15

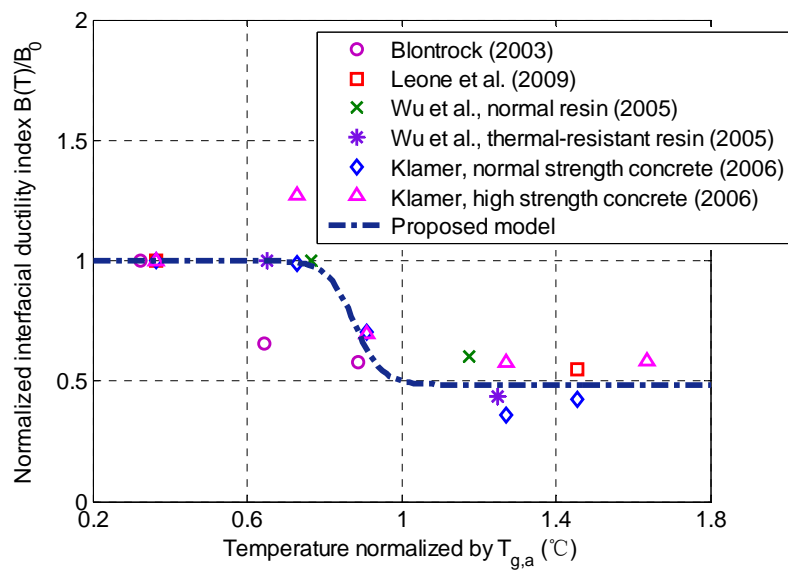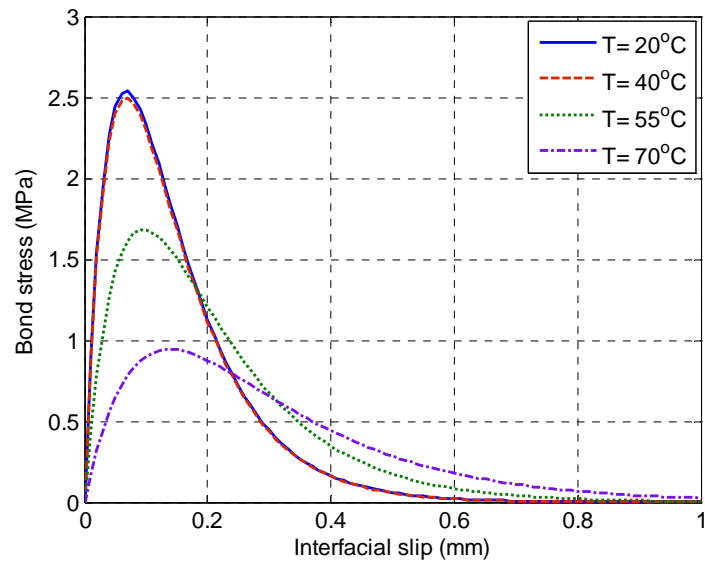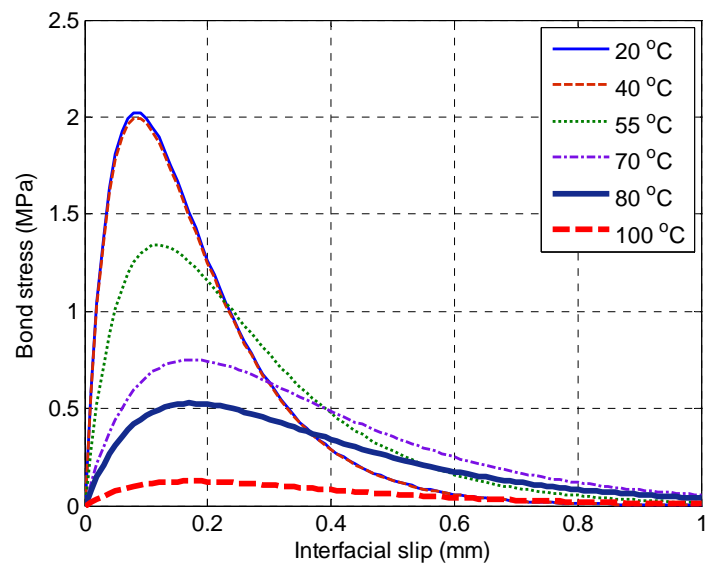**Fig. 3.** Effect of temperature on interfacial fracture energy.

Fig. 4. Effect of temperature on interfacial brittleness index.

(a) Blontrock's (2003) specimens

(b) Klamer's (2006) specimens

Fig. 5. Predicted bond-slip curves at elevated temperature.
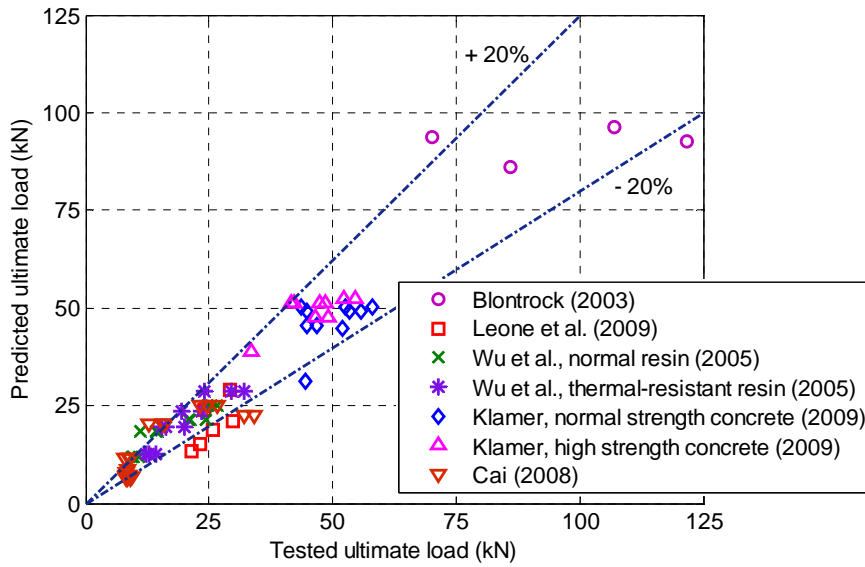
Fig. 6. Comparisons between predicted and test ultimate loads of FRP-to-concrete bonded joints at elevated temperature.
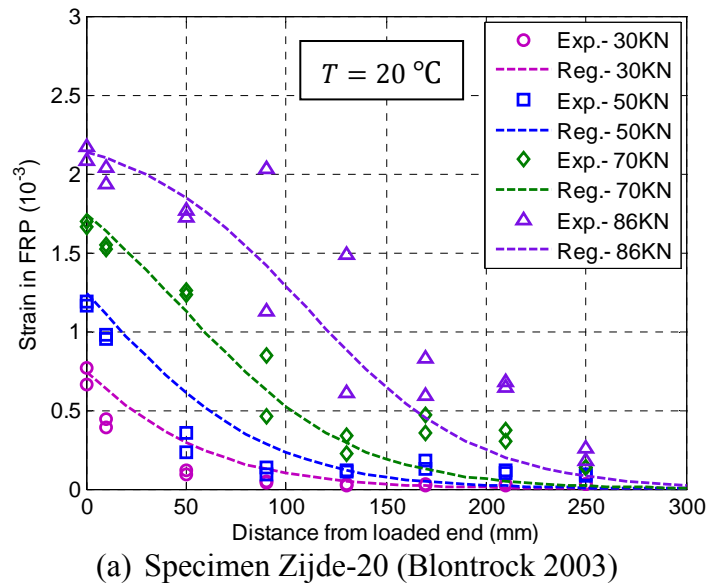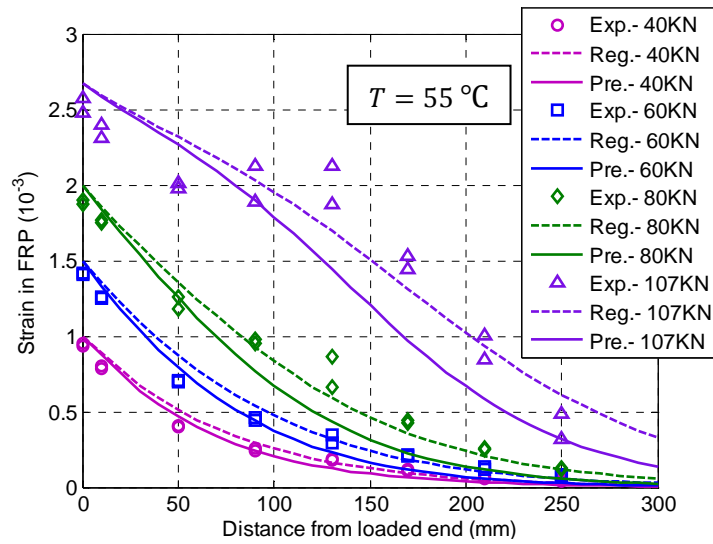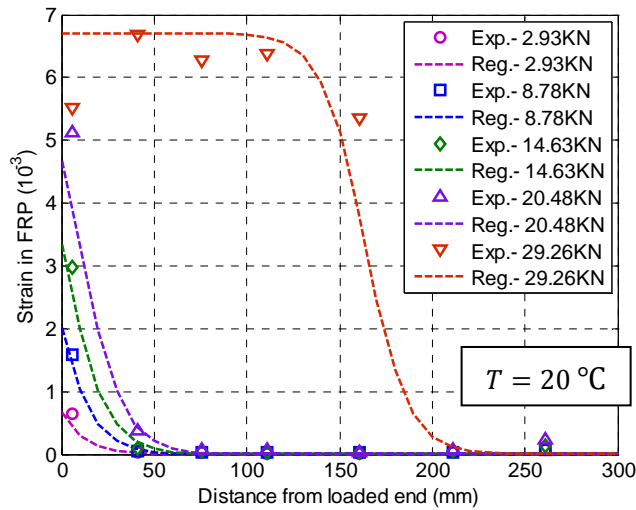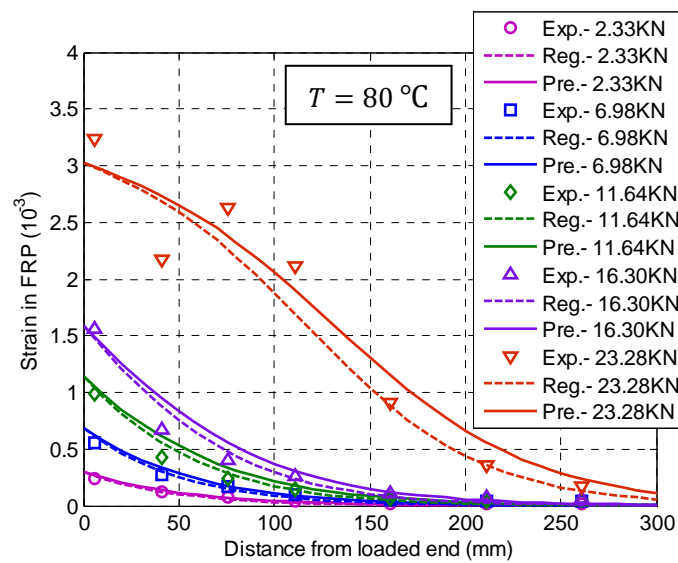

(a) Specimen Zijde-20 (Blontrock 2003)

Fig. 7. Comparisons between predicted and test strain distributions in FRP.

(b) Specimen Zijde-55 (Blontrock 2003)

(c) Specimen G-S-20 (Leone et al. 2009)

(d) Specimen G-S-80 (Leone et al. 2009)

Fig. 7. Comparisons between predicted and test strain distributions in FRP (Cont'd).

Table 1. Double-lap shear test database: specimen details and results.

Specimen name [a,b]	Temp (^{o}C)	FRP laminates					Adhesive		Bond zone		Ultimate load $P_{uT,test}$ (kN)	Failure mode [c]
		type	t_p (mm)	E_p (GPa)	f_p (MPa)	$T_{g,p}$	type	$T_{g,a}$	L (mm)	b_p (mm)		
Zijde-20	20	CFRP	1.2	165	2800	--		62	300	100	86	DB-C
Zijde-40	40	CFRP	1.2	--	--	--	Sikadur-30	62	300	100	121.6	DB-C
Zijde-55	55	CFRP	1.2	--	--	--		62	300	100	107	DB-C
Zijde-70	70	CFRP	1.2	--	--	--		62	300	100	70	DB-A
C-S-20	20	CFRP	0.117	225.6	2600	55		55	300	100	23.98	DB-C
C-S-50	50	CFRP	0.117	--	--	55	PC5800 CARBO	55	300	100	29.7	DB-C
C-S-65	65	CFRP	0.117	--	--	55		55	300	100	25.64	DB-C/A
C-S-80	80	CFRP	0.117	--	--	55		55	300	100	21.48	DB-A
C-L-20	20	CFRP	1	176	2450	--		81	300	100	80.94	DB-C/A
C-L-50	50	CFRP	1	--	--	--	PC5800 /BL	81	300	100	68.66	DB-C/A
C-L-80	80	CFRP	1	--	--	--		81	300	100	88.04	DB-C/A
G-S-20	20	GFRP	0.3	73	780	55	PC5800	55	300	100	29.26	DB-C
G-S-80	80	GFRP	0.3	--	--	55	CARBO	55	300	100	23.28	DB-A
O-26	26	CFRP	0.111	235	3400	34		34	200	50	26.6	DB-C
O-26	26	CFRP	0.111	235	3400	34		34	200	50	25.55	DB-C
O-26	26	CFRP	0.111	235	3400	34		34	200	50	24.5	DB-C
O-30	30	CFRP	0.111	--	--	34		34	200	50	24.3	DB-C
O-30	30	CFRP	0.111	--	--	34		34	200	50	21.25	DB-C
O-30	30	CFRP	0.111	--	--	34	Normal epoxy resin	34	200	50	20.75	DB-A
O-40	40	CFRP	0.111	--	--	34		34	200	50	14.6	DB-A
O-40	40	CFRP	0.111	--	--	34		34	200	50	14.15	DB-A
O-40	40	CFRP	0.111	--	--	34		34	200	50	11.15	DB-A
O-50	50	CFRP	0.111	--	--	34		34	200	50	10.85	DB-A
O-50	50	CFRP	0.111	--	--	34		34	200	50	9.65	DB-A
O-50	50	CFRP	0.111	--	--	34		34	200	50	9.35	DB-A
T-26	26	CFRP	0.111	235	3400	55		40	200	50	32.2	DB-C
T-26	26	CFRP	0.111	235	3400	55		40	200	50	29.55	DB-C
T-26	26	CFRP	0.111	235	3400	55		40	200	50	24.05	DB-C
T-40	40	CFRP	0.111	--	--	55		40	200	50	23.55	DB-C
T-40	40	CFRP	0.111	--	--	55		40	200	50	23.54	DB-A
T-40	40	CFRP	0.111	--	--	55	Thermo-resistant epoxy resin	40	200	50	19.35	DB-A
T-50	50	CFRP	0.111	--	--	55		40	200	50	19.95	DB-A
T-50	50	CFRP	0.111	--	--	55		40	200	50	16.25	DB-A
T-50	50	CFRP	0.111	--	--	55		40	200	50	15.35	DB-A
T-60	60	CFRP	0.111	--	--	55		40	200	50	14.25	DB-A
T-60	60	CFRP	0.111	--	--	55		40	200	50	12.85	DB-A
T-60	60	CFRP	0.111	--	--	55		40	200	50	12.1	DB-A
B1-20	20	CFRP	1.2	165	2800	62		62	300	50	44.71	DB-C
B1-20	20	CFRP	1.2	165	2800	62		62	300	50	46.69	DB-C
B1-40	40	CFRP	1.2	--	--	62	Sikadur-30	62	300	50	44.89	DB-C
B1-50	50	CFRP	1.2	--	--	62		62	300	50	43.51	DB-C
B1-50	50	CFRP	1.2	--	--	62		62	300	50	52.69	DB-C
B1-50	50	CFRP	1.2	--	--	62		62	300	50	58.11	DB-C

Table 1. (Continued)

B1-70	70	CFRP	1.2	--	--	62		62	300	50	55.82	DB-A
B1-70	70	CFRP	1.2	--	--	62		62	300	50	53.36	DB-A
B1-80	80	CFRP	1.2	--	--	62		62	300	50	51.86	DB-A
B1-100	100	CFRP	1.2	--	--	62		62	300	50	44.54	DB-A
B2-20	20	CFRP	1.2	165	2800	62		62	300	50	49.16	DB-C
B2-20	20	CFRP	1.2	165	2800	62		62	300	50	46.59	DB-C
B2-40	40	CFRP	1.2	--	--	62	Sikadur-30	62	300	50	48.52	DB-C
B2-40	40	CFRP	1.2	--	--	62		62	300	50	47.33	DB-C
B2-50	50	CFRP	1.2	--	--	62		62	300	50	54.62	DB-C
B2-50	50	CFRP	1.2	--	--	62		62	300	50	52.38	DB-C
B2-70	70	CFRP	1.2	--	--	62		62	300	50	41.56	DB-A
B2-70	70	CFRP	1.2	--	--	62		62	300	50	42.31	DB-A
B2-90	90	CFRP	1.2	--	--	62		62	300	50	33.46	DB-A
CS-4	4	CFRP	0.165	260	2900	50		50	120	80	26.7	DB-C
CS-4	4	CFRP	0.165	260	2900	50		50	120	80	23.2	DB-C/A
CS-4	4	CFRP	0.165	260	2900	50		50	120	80	24.6	DB-C
CS-40	40	CFRP	0.165	--	--	50		50	120	80	34.2	DB-C
CS-40	40	CFRP	0.165	--	--	50		50	120	80	34.0	DB-C
CS-40	40	CFRP	0.165	--	--	50		50	120	80	32.0	DB-C
CS-60	60	CFRP	0.165	--	--	50		50	120	80	15.9	DB-A
CS-60	60	CFRP	0.165	--	--	50		50	120	80	15.8	DB-A
CS-60	60	CFRP	0.165	--	--	50		50	120	80	12.8	DB-A
CS-80	80	CFRP	0.165	--	--	50		50	120	80	8.0	DB-A
CS-80	80	CFRP	0.165	--	--	50		50	120	80	9.1	DB-A
CS-80	80	CFRP	0.165	--	--	50	HM 300	50	120	80	8.8	DB-A
CS-100	100	CFRP	0.165	--	--	50		50	120	80	8.7	DB-A
CS-100	100	CFRP	0.165	--	--	50		50	120	80	8.1	DB-A
CS-100	100	CFRP	0.165	--	--	50		50	120	80	8.5	DB-A
CS-120	120	CFRP	0.165	--	--	50		50	120	80	8.3	DB-A
CS-120	120	CFRP	0.165	--	--	50		50	120	80	8.6	DB-A
CS-120	120	CFRP	0.165	--	--	50		50	120	80	9.2	DB-A
CS-140	140	CFRP	0.165	--	--	50		50	120	80	8.3	DB-A
CS-140	140	CFRP	0.165	--	--	50		50	120	80	9.3	DB-A
CS-140	140	CFRP	0.165	--	--	50		50	120	80	8.3	DB-A
CS-160	160	CFRP	0.165	--	--	50		50	120	80	8.2	DB-A
CS-180	180	CFRP	0.165	--	--	50		50	120	80	8.4	DB-A

[a] Some of the specimen names are assigned by the present authors as they are not available in the original papers.

[b] Specimens Zijde-20 to Zijde-70 are from Blontrock (2003); Specimens C-S-20 to G-S-80 are from Leone et al. (2009); Specimens O-26 to T-60 are from Wu et al. (2005); Specimens B1-20 to B2-90 are from Klamer (2006); Specimens CS-4 to CS-180 are from Cai (2008). Note that specimens B1-20 to B1-100 were prepared with normal strength concrete whereas specimens B2-20 to B2-90 were prepared with high strength concrete.

[c] Failure mode: DB-C = Debonding failure in the concrete substrate; DB-A = Debonding failure within the adhesive layer or at the adhesive/concrete interface; DB-C/A = DB-C and DB-A were both observed.

Table 2 Summary of predicted results for the test specimens.

Specimen name	FRP laminates $E_p^{\ d}$ (GPa)	ΔP (kN)	$P_{uT,test}$ - ΔP	G_f (N/mm)	A (10^{-2})	B (mm^{-1})	Ultimate load	
							$P_{uT,pred}$	$P_{uT,pred}$ /$P_{uT,test}$
Zijde-20	165	0	86.00	0.493	0.229	10.29	85.93	1.00
Zijde-40	164.47	7.474	114.13	0.871	0.305	6.75	92.76	0.76
Zijde-55	164.31	13.068	93.93	0.591	0.252	5.96	96.23	0.90
Zijde-70	164.11	18.646	51.35	0.177	0.138	--	93.67	1.34
C-S-20	225.6	0	23.98	0.274	0.454	--	23.95	1.00
C-S-50	164.62	1.149	28.55	0.532	0.742	--	20.91	0.70
C-S-65	164.46	1.723	23.92	0.374	0.621	--	18.85	0.74
C-S-80	164.46	2.297	19.18	0.240	0.498	--	13.28	0.62
G-S-20	73	0	29.26	0.492	0.671	12.78	29.23	1.00
G-S-80	52.22	0.381	22.90	0.359	0.672	6.98	15.31	0.66
O-26	235	0	26.60	1.364	1.026	--	25.19	0.95
O-26	235	0	25.55	1.259	0.985	--	25.19	0.99
O-26	235	0	24.50	1.157	0.945	3.67	25.19	1.03
O-30	171.59	0.076	24.22	1.549	1.279	--	21.26	0.86
O-30	171.59	0.076	21.17	1.184	1.118	--	21.26	1.00
O-30	171.59	0.076	20.67	1.129	1.092	--	21.26	1.03
O-40	171.32	0.265	14.34	0.543	0.757	2.21	18.62	1.28
O-40	171.32	0.265	13.89	0.509	0.733	--	18.62	1.32
O-40	171.32	0.265	10.89	0.313	0.575	--	18.62	1.67
O-50	171.32	0.454	10.40	0.286	0.549	--	11.74	1.08
O-50	171.32	0.454	9.20	0.223	0.486	--	11.74	1.22
O-50	171.32	0.454	8.90	0.209	0.470	--	11.74	1.26
T-26	235	0	32.20	1.999	1.242	3.81	28.60	0.89
T-26	235	0	29.55	1.683	1.139	--	28.60	0.97
T-26	235	0	24.05	1.115	0.927	--	28.60	1.19
T-40	176.76	0.273	23.28	1.387	1.192	--	23.74	1.00
T-40	176.76	0.273	23.27	1.386	1.191	--	23.74	1.00
T-40	176.76	0.273	19.08	0.931	0.977	--	23.74	1.23
T-50	171.48	0.455	19.50	1.003	1.029	--	19.52	0.98
T-50	171.48	0.455	15.80	0.658	0.833	--	19.52	1.20
T-50	171.48	0.455	14.90	0.585	0.786	1.67	19.52	1.27
T-60	171.32	0.644	13.61	0.489	0.719	--	12.49	0.88
T-60	171.32	0.644	12.21	0.393	0.645	--	12.49	0.97
T-60	171.32	0.644	11.46	0.347	0.605	--	12.49	1.03
B1-20	165	0	44.71	0.521	0.233	8.28	45.67	1.02
B1-20	165	0	46.69	0.569	0.244	8.15	45.67	0.98
B1-40	164.47	3.78	41.11	0.442	0.215	8.10	49.11	1.09
B1-50	164.37	5.67	37.84	0.375	0.198	8.29	50.44	1.16
B1-50	164.37	5.67	47.02	0.579	0.246	6.07	50.44	0.96
B1-50	164.37	5.67	52.44	0.720	0.275	3.00	50.44	0.87
B1-70	164.18	9.44	46.38	0.564	0.243	4.11	49.31	0.88
B1-70	164.18	9.44	43.92	0.506	0.230	1.75	49.31	0.92

Table 2. (Continued)

B1-80	163.94	11.32	40.54	0.431	0.213	3.49	44.69	0.86
B1-100	163.50	15.05	29.49	0.229	0.155	--	31.30	0.70
B2-20	165	0	49.16	0.628	0.255	7.39	47.85	0.97
B2-20	165	0	46.59	0.564	0.242	7.68	47.85	1.03
B2-40	164.47	3.80	44.72	0.521	0.233	10.67	51.29	1.06
B2-40	164.47	3.80	43.53	0.494	0.227	8.49	51.29	1.08
B2-50	164.37	5.70	48.92	0.624	0.255	3.37	52.60	0.96
B2-50	164.37	5.70	46.68	0.568	0.243	7.12	52.60	1.00
B2-70	164.11	9.48	32.08	0.269	0.167	--	51.26	1.23
B2-70	164.11	9.48	32.83	0.281	0.171	4.35	51.26	1.21
B2-90	163.74	13.24	20.22	0.107	0.106	4.42	39.00	1.17
CS-4	260	0	26.70	0.328	0.393	--	24.87	0.93
CS-4	260	0	23.20	0.247	0.341	--	24.87	1.07
CS-4	260	0	24.60	0.278	0.362	--	24.87	1.01
CS-40	191.08	1.77	32.43	0.661	0.653	--	22.65	0.66
CS-40	191.08	1.77	32.23	0.653	0.649	--	22.65	0.67
CS-40	191.08	1.77	30.23	0.575	0.608	--	22.65	0.71
CS-60	189.54	2.75	13.15	0.109	0.265	--	20.21	1.27
CS-60	189.54	2.75	13.05	0.107	0.263	--	20.21	1.28
CS-60	189.54	2.75	10.05	0.063	0.202	--	20.21	1.58
CS-80	189.54	3.74	4.26	0.011	0.086	--	11.61	1.45
CS-80	189.54	3.74	5.36	0.018	0.108	--	11.61	1.28
CS-80	189.54	3.74	5.06	0.016	0.102	--	11.61	1.32
CS-100	189.54	4.72	3.38	0.007	0.068	--	7.06	0.87
CS-100	189.54	4.72	3.98	0.010	0.080	--	7.06	0.81
CS-100	189.54	4.72	3.78	0.009	0.076	--	7.06	0.83
CS-120	189.54	5.71	2.59	0.004	0.052	--	6.36	0.77
CS-120	189.54	5.71	2.89	0.005	0.058	--	6.36	0.74
CS-120	189.54	5.71	3.49	0.008	0.070	--	6.36	0.69
CS-140	189.54	6.69	1.61	0.002	0.032	--	6.87	0.83
CS-140	189.54	6.69	2.61	0.004	0.053	--	6.87	0.74
CS-140	189.54	6.69	1.61	0.002	0.032	--	6.87	0.83
CS-160	189.54	7.67	0.53	0.0002	0.011	--	7.72	0.94
CS-180	189.54	8.66	-0.26	-0.00004	-0.005	--	8.67	1.03
							Mean	1.01

[d] The elastic modulus degradation of prefabricated FRP plates was evaluated using Bisby's (2003) model: $E_{pT}/E_{p0} = (1 - a_1)/2 \times \tanh(-a_2 \times (T - a_3)) + (1 + a_1)/2$; for CFRP plates: a_1 =0.05, a_2 =8.68×10^{-3}, a_3 =367.41; for GFRP plates: a_1=0.05, a_2 =7.91×10^{-3}, a_3 =320.35. The elastic modulus degradation of FRP sheets was evaluated using the present proposed model : $E_{pT}/E_{p0} = (1 - a_1)/2 \times \tanh(-a_2 \times (T/T_g - a_3)) + (1 + a_1)/2$, where a_1=0.729, a_2 =9.856, a_3 =0.607.